Compositional ordering in relaxor ferroelectric $Pb(BB')O_3$: Nearest neighbor approach

J. Zhang,[1] L. Liu,[2] A. A. Bokov,[3] N. Zhang,[4] D. Wang,[1,*] Z.-G. Ye,[3,†] and C.-L. Jia[1,5]

[1]*School of Microelectronics & State Key Laboratory for Mechanical Behavior of Materials, Xi'an Jiaotong University, Xi'an 710049, China*

[2]*College of Materials Science and Engineering, Guilin University of Technology, Guilin 541004, China*

[3]*Department of Chemistry and 4D LABS, Simon Fraser University, Burnaby, British Columbia V5A 1A6, Canada*

[4]*Electronic Materials Research Laboratory–Key Laboratory of the Ministry of Education and International Center for Dielectric Research, Xi'an Jiaotong University, Xi'an 710049, China*

[5]*Ernst Ruska Center for Microscopy and Spectroscopy with Electrons, Research Center Jülich, D-52425 Jülich, Germany*

(Received 27 June 2020; revised 31 January 2021; accepted 1 February 2021; published 17 February 2021)

Relaxor ferroelectrics, which form a peculiar class of functional materials, are often composed of complex perovskites $Pb(BB')O_3$, as represented by $Pb(Mg_{1/3}Nb_{2/3})O_3$ where the compositional ordering of Mg and Nb is believed to be essential to its relaxor properties. In this work, analysis using a first-principles-based model shows that, while the electrostatic interactions are important, the nearest neighbor assumption, which was used for metallic alloys, can be adopted to understand the compositional ordering in $Pb(BB')O_3$. Numerical simulations with the Kawasaki Monte Carlo method can model the experimentally observed compositional ordering by maximizing the number of the unlike B-B' pairs (or the Bethe's parameter), which is the overriding factor that determines the ordering. Subtle points of configuration energy degeneracy are also discussed, which explains the partial disorder inherently present in such systems.

DOI: 10.1103/PhysRevB.103.054201

Complex perovskites of general formulas $A(BB')O_3$ are actively sought after to achieve specific properties such as relaxor ferroelectricity with high dielectric constant and excellent electromechanical response. One of the canonical relaxor ferroelectric materials is $Pb(Mg_{1/3}Nb_{2/3})O_3$ (PMN) [1–4]. The ordering (disordering) of the cations on the B site has crucial influence on their properties. For instance, it has been argued that fully ordered perovskites cannot be true relaxors [5,6] and a change in the compositional order parameter can change dramatically the ferroelectric or relaxor properties [7,8]. The ordering/disordering problem has been studied intensively in the last few decades [9–11], but remains a puzzling issue. Some recent studies include the use of transmission electron microscopy (TEM) to show gradient ordering in PMN [12] and the examination of the relaxor behavior in ordered PMN thin films [13]. However, the reason why PMN possesses alternating (111) planes is obscure to many researchers, especially when the Coulomb interaction between the B and B' ions is emphasized [11,14,15]. In contrast, the nearest neighbor approach established in this work provides a clear-cut explanation of this unique phenomenon associated with relaxor physics.

The determination of complex perovskite structure is a challenging task. Experimentally, the compositional ordering can be determined with x-ray, neutron, or electron diffraction [16]. While it is generally realized that the more different the size and charge of B and B' are, the more likely $A(BB')O_3$ has an ordered structure, a quantitative understanding of the compositional ordering is not fully achieved yet. For instance, despite some degrees of disorder, it is found that a great portion of PMN (and similar systems) has the rocksalt configuration where one layer of Nb alternates with another layer of mixed Nb and Mg along the ⟨111⟩ direction and there exist the β^{I} and β^{II} sublattices [12,13]. Interestingly, many other systems with the 1:1 cation ratio, such as $Pb(Sc_{1/2}Nb_{1/2})O_3$, also have this feature [17], giving rise to the universal β^{I} and β^{II} sublattices [16]. This unique phenomenon strongly indicates that an underlying principle exists, which can quantitatively and simply explain the special compositional structure. Revealing such a principle requires a computationally tractable model based on first-principle calculations.

If we strip the Pb and O atoms from the system, the remainder of $Pb(BB')O_3$ is nothing but a binary alloy, which has been investigated using the *nearest neighbor assumption* (NNA) by Bragg, Williams, and Bethe [18,19]. Given the similarity, it is sensible to consider the NNA in the modeling of $Pb(BB')O_3$. In fact, Welberry built models to simulate scattering data [20], based on the NNA without considering the long-range Coulomb interactions. Bokov et al showed that the temperature dependence of the compositional order parameter, s, of $Pb(Yb_{0.5}Nb_{0.5})O_3$, derived based on the NNA, can well fit the experimental data [9]. On the other hand, since B and B' (e.g., Mg^{2+} and Nb^{5+} in PMN) have different valence states, their Coulomb interactions cannot be ignored [11]. Can such different approaches both be applied to understand the ordering in complex perovskites? Here, we show that both perspectives are needed to model $Pb(BB')O_3$ accurately and predict its compositional ordering. We find that, while the

*dawei.wang@xjtu.edu.cn
†zye@sfu.ca

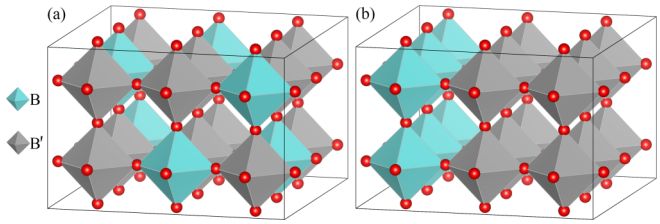

FIG. 1. Two configurations with different distribution of the B and B' ions are shown in (a) and (b). The Pb ions have been omitted for clarity.

electrostatic energy is strong, the NNA can be adopted, which implies that maximizing the number of unlike pairs (B-B') explains the compositional ordering.

We use both the NNA and the Coulomb energy [11] to model the total energy:

$$E_{\text{total}} = E_0 + E_{\text{NNA}} + E_{\text{cc}}, \tag{1}$$

where E_0 is the background energy independent of compositional ordering, and $E_{\text{NNA}} = \tilde{\epsilon}_{BB'}N_{BB'} + \tilde{\epsilon}_{BB}N_{BB} + \tilde{\epsilon}_{B'B'}N_{B'B'}$ is the NNA energy arising when two unit cells are put as nearest neighbors (NNs). Omitting Pb and O, there are two types of like pairs (B-B, B'-B') and one type of unlike pair (B-B') (see Fig. 1), and their numbers are denoted by N_{BB}, $N_{B'B'}$, and $N_{BB'}$, respectively. $\tilde{\epsilon}$ is the "bare" short-range energy between pairs; later we will also define $\epsilon_{BB'}$, which includes the Coulomb contribution from neighboring B and B' ions. $E_{\text{cc}} = \sum_{ij} Q_{ij}\Delta q_i \Delta q_j$ is the Coulomb energy, where Q_{ij} is the Ewald Coulomb matrix element connecting the ith and jth charges [21] and Δq_i is the effective charge of the B or B' ion on site i. In a $Pb(B_{1/3}B'_{2/3})O_3$ compound, to ensure the electric neutrality, we assume that the effective charge of B is $\Delta q_B = -2q_0$ and $\Delta q_{B'} = q_0$ for B'.

The numbers of pairs are not independent since [18] $N_{BB} = 3N_B - 0.5N_{BB'}$ and $N_{B'B'} = 3N_{B'} - 0.5N_{BB'}$, only one of them being the independent variable (here we choose $N_{BB'}$). Therefore, the total energy is

$$E_{\text{total}} = E'_0 + \sum_{ij} Q_{ij}\Delta q_i \Delta q_j + \epsilon'_{BB'}N_{BB'}, \tag{2}$$

where $\epsilon'_{BB'}$ defines the NN interaction and the second Coulomb term has been used in the electrostatic model [11].

The parameters in Eq. (2) can be obtained by fitting *ab initio* results. We use SUPERCELL [22] to generate a series of $3 \times 3 \times 2$ PMN and $Pb(Cd_{1/3}Nb_{2/3})O_3$ (PCN) supercells with their lattice constants set to be the experimental values ($a_{\text{PMN}} = 4.040$ Å and $a_{\text{PCN}} = 4.138$ Å), and perform *ab initio* computation to obtain their energies, which are then used to extract the parameters by fitting. The SUPERCELL automatically generates symmetry nonequivalent configurations, resulting in 178 different $3 \times 3 \times 2$ supercells with energies distributed over a wide range. All *ab initio* calculations are performed with GPAW [23] using plane waves (PWs) with a cutoff energy of 750 eV, a $3 \times 3 \times 4$ Brillouin-zone sampling grid [24], and the Perdew-Burke-Ernzerhof (PBE) exchange-correlation functional [25]. The fitting uses the least-square method from SCIPY [26].

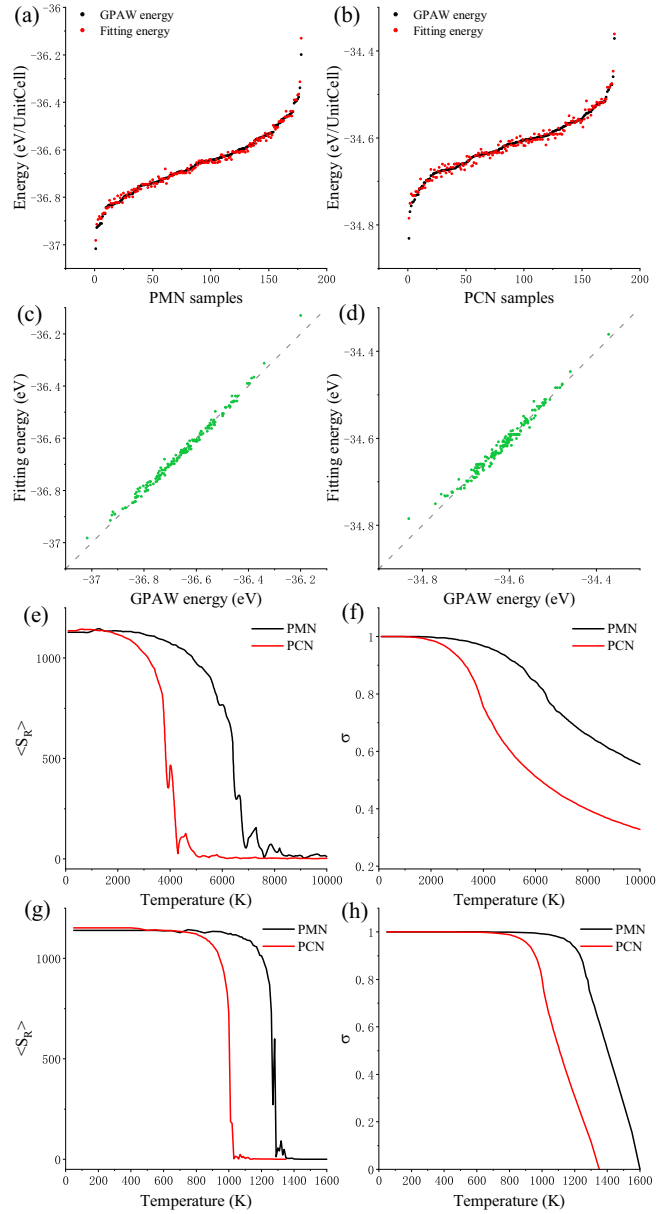

FIG. 2. The fitting results (red dots) are compared to the GPAW calculation results (black dots) for PMN (a) and PCN (b). The accuracy of the fitting is demonstrated for PMN (c) and PCN (d) by plotting the fitting energy against the GPAW energy. In (e) and (f), the order parameters of $\langle S_R \rangle$ and the Bethe's parameter σ versus temperature are shown, while (g) and (h) show the results after the melting temperature is used to refine the theory.

Figures 1(a) and 1(b) show the configurations with the lowest and highest energies, respectively. Table II shows the parameters for PMN and PCN obtained by the fitting as shown in Figs. 2(a) and 2(b). Figures 2(c) and 2(d) compare the GPAW results to its fitting, showing that the model of Eq. (2) is adequate. The parameters shown in Table I are not sensitive to the lattice parameter. For instance, the same calculation for PMN with a lattice constant of 4.08 Å (the extrapolated high-temperature value) results in similar values for the parameters. We note that fitting results (not shown here) with only the long-range energy or the short-range energy for PMN are

TABLE I. Fitting results for PCN and PMN using a $3 \times 3 \times 2$ supercell. Note that $\epsilon_{BB'}$ is not a direct fitting parameter, as discussed in the text.

Parameter	E_0' (eV)	q_0 ($\|e\|$)	$\epsilon'_{BB'}$ (eV)	$\epsilon_{BB'}$ (eV)
PCN	−616.713	0.1672	−0.19043	−0.52512
PMN	−648.309	0.2763	−0.28393	−1.22052

reduced in accuracy, indicating the importance of including both the long-range and short-range interactions.

Having obtained the parameters, we use the Monte Carlo (MC) Kawasaki algorithm [27] to numerically obtain the compositional ordering of PMN and PCN on a $12 \times 12 \times 12$ supercell (1728 unit cells), and gradually cool down the system from 10 000 to 100 K with a step of 100 K. At each temperature, we sweep the system 20 000 times, and in each sweep, we try to exchange each B (B') with a randomly selected B' (B) ion, and decide whether or not to accept the exchange according to the energy change. In total, at each temperature, $20\,000 \times 1728$ attempted exchanges are made. A typical simulation result for PCN (or PMN) is shown in Fig. 3(a) where two types of atom columns can be seen along the ⟨110⟩ direction. The alternating structure becomes obvious when the columns are shown differently according to whether they contain all Nb ions or a mixture with more than two of the minority ion (Cd for PCN, or Mg for PMN) in Fig. 3(b), which constitute the β^{I} and β^{II} B-site sublattices [12,13].

Given the special ⟨110⟩ columns and the (111) planes, we calculate the long-range order parameter, i.e., the R-point averaged sum:

$$S_R = \sum_i \sigma_i (-1)^{i_x + i_y + i_z},$$

where $\sigma = 1$ for Nb and $\sigma = -1$ for Cd (or Mg), and i_x, i_y, and i_z are the x, y, and z coordinates of the ith site. For each temperature, we collect many snapshots of the configuration and calculate S_R for each of them, which are then averaged to obtain $\langle S_R \rangle$. Figure 2(e) shows that $\langle S_R \rangle$ undergoes sudden changes at 6000 and 4000 K for PMN and PCN, respectively, which signifies a compositional order-disorder phase transition.

It is commonly believed that the major driving forces responsible for compositional ordering in perovskites arise from the differences in the valence and size of the mixed ions [28] so that the order-disorder transition temperature should be higher in those $Pb(B_{1/3}B'_{2/3})O_3$ perovskites in which the ionic radius difference, $\Delta R = |R_B - R_{B'}|$, is larger. However, it was also suggested that, in contrast, the difference in ionic sizes is not a significant factor [29]. Our calculations agree with this suggestion. Indeed, given $R_{\mathrm{Nb}} = 0.64$ Å, $R_{\mathrm{Mg}} = 0.72$ Å, and $R_{\mathrm{Cd}} = 0.95$ Å [30], $\Delta R = 0.36$ Å for PCN is significantly larger than $\Delta R = 0.08$ Å for PMN, while the transition temperature is significantly smaller [Fig. 2(e)].

We now discuss the underlying principle that generates the typical configurations reported for PMN and other similar relaxor ferroelectrics [31,32] from the energy point of view. The Coulomb energy in Eq. (2) can be split into two parts: the NN part and the rest. For the NN part, there are only three types: $Q_{01}\Delta q_B \Delta q_B$, $Q_{01}\Delta q_{B'}\Delta q_{B'}$, and $Q_{01}\Delta q_B \Delta q_{B'}$, where Q_{01} is

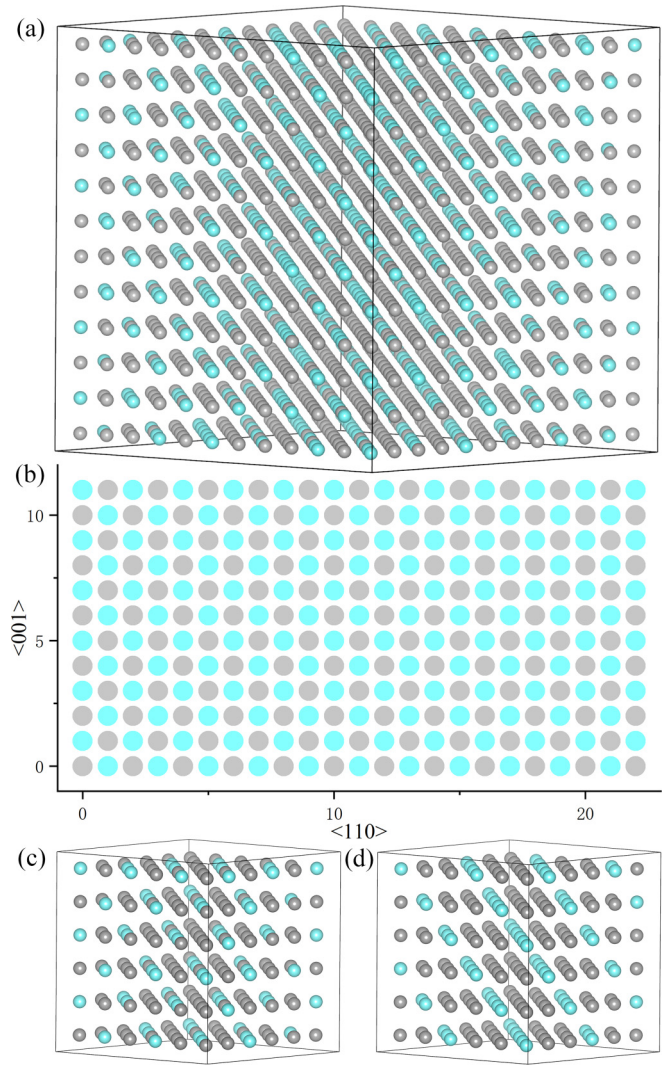

FIG. 3. (a) Some ⟨110⟩ columns that contain only Nb (grey) form a series of (111) planes, which alternate with planes containing both Cd (or Mg) (blue) and Nb. (b) Projection along one [110] direction shows alternating columns as type I ($N_{\mathrm{Cd}} \geqslant 3$) or type II ($N_{\mathrm{Cd}} < 3$) lattices. Two low-energy configurations, which are denoted as 1:1 (c) and 1:2 (d), both have special (111) planes.

the Ewald matrix element for the NN Coulomb interaction [21]. Given the fact that only $N_{BB'}$ is independent, the total energy can be converted to

$$E_{\mathrm{total}} = E_0'' + \sum_{ij}{}' Q_{ij}\Delta q_i \Delta q_j + \epsilon_{BB'} N_{BB'}, \tag{3}$$

where $'$ in the $\sum'$ indicates a sum without NN and $\epsilon_{BB'} = \epsilon'_{BB'} - 9Q_{01}q_0^2$ and its value is shown in Table I for the $12 \times 12 \times 12$ supercell. We have verified that for PMN and PCN the Coulomb energy excluding the NN part is smaller than the others including both the NN Coulomb interaction and the E_{NNA} term (the former is about 10% of the latter for the low-in-energy configurations).

The above analysis demonstrates the significance of the NNA when the second term in Eq. (3), which is relatively small, is omitted. It reveals an interesting situation where the

TABLE II. The energies of PMN corresponding to the two configurations shown in Figs. 3(c) and 3(d), where $E_0 = -35.1392$ eV is the same for both.

Configuration	1:2	1:1
NN (eV)	−1.8848	−1.8848
Coulomb energy excluding NN (eV)	0.0369	0.0547
Sum (eV)	−1.8479	−1.8301

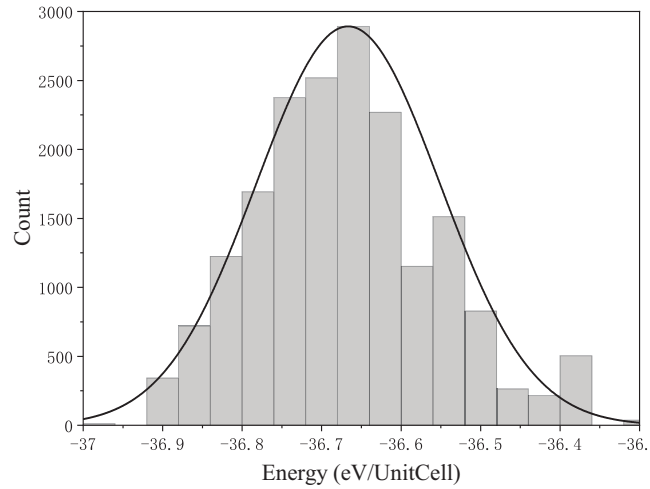

FIG. 4. Energy configuration statistics of PMN for $3 \times 3 \times 2$ supercells. There are a total of 18 564 different configurations (including symmetrically equivalent ones), and the structures with the lowest energy only make up a small fraction.

NN interaction [the last term in Eq. (3)] can still dominate the energy even when the Coulomb interaction is included. In his seminal work on metallic alloys [33], Bethe introduced an order parameter $\sigma = [q - q(\text{rand})]/[q(\text{max}) - q(\text{rand})]$ where $q = N_{BB'}/N$ is the fraction of the unlike pairs among all the NN pairs. For perfect and random order, q has the values $q(\text{max})$ and $q(\text{rand})$, respectively. For $Pb(B_{1/3}B'_{2/3})O_3$, we have $q(\text{max}) = 2/3$ and $q(\text{rand}) = 4/9$, and the order parameter becomes $\sigma = 9q/2 - 2$ [34]. The virtue of using the Bethe's parameter is that no prior information regarding ordering is needed, unlike S_R, to obtain the relation between the ordering parameter and temperature [see Fig. 2(f)].

It is easy to prove that minimizing the formation energy in Eq. (3) requires maximizing σ, which is achieved by implying the NNA. Configurations with maximal σ indeed appear in our MC simulations with two examples shown in Figs. 3(c) and 3(d) for a $6 \times 6 \times 6$ supercell, both of which have $\sigma = 1$ ($q = 2/3$) with 432 B-B' pairs, although the 1:2 configuration in Fig. 3(d) is extremely rare to be seen. Locally or globally maximizing the Bethe's parameter thus constitutes a principle to understand the compositional ordering in $Pb(B_{1/3}B'_{2/3})O_3$, consistent with the experimental findings that the special $\langle 110 \rangle$ columns or (111) planes are often observed [12,14]. The parallel between complex oxides (e.g., PMN and PCN) and binary metallic alloys regarding compositional ordering is remarkable.

The implication of NNA also reveals the configuration degeneracy which in turn explains why perfect ordering is often hard to achieve in $Pb(B_{1/3}B'_{2/3})O_3$. For instance, the two configurations shown in Figs. 3(c) and 3(d) have exactly the same energy (see Table II) if only the NN interaction is included. However, comparing to a simple 1:1 binary metallic alloy, $Pb(B_{1/3}B'_{2/3})O_3$ can exhibit more variants in terms of configuration as they can (i) exchange B and B' cations in the β^{II} columns, and (ii) form domain boundaries [12], due to the antiphase (or "out-of-step") domains [18] without changing the number of unlike pairs. The degenerate configurations under NNA can only be distinguished by considering the Coulomb interaction beyond the NNs, which is smaller as demonstrated in Table II. Interestingly, the results in Table II also indicate that, if only the Coulomb interaction is included, the 1:2 structure will be preferred because of its lower energy.

It is worth noting that the non-NN Coulomb energy has an opposite trend to the NN energies, implying these two types of energies compete with each other. As a matter of fact, our simulations show that if the Coulomb interactions beyond the NN are removed, the order-disorder transition temperature will increase to 24 000 and 10 000 K for PMN and PCN, respectively, indicating that non-NN Coulomb interaction prevents the ordered configurations from forming. This can be understood by the fact that the first and second NN Coulomb interactions both favor unlike pairs, effectively working against each other and making the ordering more difficult.

We note that the lowest-in-energy configuration is not often found in experiments (or in our simulations) due to the entropy related to the number of equivalent configurations. For instance, there are only a few equivalent states for the 1:2 configuration with a perfect long-range order as shown in Fig. 3(d), while there are many more for the 1:1 configuration as shown in Fig. 3(c). By enumerating every possible configuration, we plot the distribution of configurations for the $3 \times 3 \times 2$ supercell (see Fig. 4). Even with such a small supercell, the number of configurations at the lowest energy can be much smaller than at a higher energy, indicating that the entropy is also a factor determining the final configuration, which explains why partially disordered configurations are often observed in PMN.

Moreover, we have studied a few other well-known relaxor ferroelectrics, and find that their $\epsilon_{BB'}$ are all negative. Such results are not accidental because it is a necessary condition to form the complex perovskites with mixed occupancy on the B site. It will be interesting to find ion pairs with positive $\epsilon_{BB'}$. Such pairs, if they exist, may be used (e.g., by substitution) to tune the ionic distribution or configuration in a complex perovskite.

Figures 2(e) and 2(f) show that the the predicted order-disorder transition temperature is quite high, which is most likely due to the fact that the *ab initio* calculations (with GPAW in our case) can only provide 0 K results, not taking into account the kinetic energy of ions. At a finite temperature, the energy spreading [see Figs. 2(a) and 2(b)] could be smaller, which will lead to smaller fitting parameters and a lower transition temperature. We can resolve this issue phenomenologically by employing the melting temperature as a reference and predict the order-disorder transition temperature.

In order to include the influence of finite temperature, we focus on the high-temperature end and use the Dulong-Petit law [35] to determine the binding energy at a finite temperature T by

$$E_B(T) = E_0 - Nk_BT, \tag{4}$$

where E_0 is the energy at 0 K calculated by GPAW and Nk_BT is the kinetic energy. Since the actual degree of freedom contributing to the kinetic energy is not reliably known, the parameter N needs to be determined using additional information. Equation (4) shows that the binding energy decreases with temperature; at the melting temperature T_m, the material will break down and thus $E_B(T_m) \simeq 0$, leading to

$$E_B(T) = E_0\Big(1 - \frac{T}{T_m}\Big). \tag{5}$$

Given this additional constraint set by the melting temperature, it is natural that the fitting parameters in Eq. (2) will scale with the temperature as $q_0(T) = q_0\sqrt{1 - T/T_m}$ and $\varepsilon'_{BB'}(T) = \varepsilon'_{BB'}(1 - T/T_m)$. In essence, such variations of the fitting parameters are the results of the energy landscape (with respect to the 178 alloy configurations) changing with temperature.

With the temperature-dependent parameters, we again performed MC simulations for PMN and PCN with the melting temperatures of 1600 [36] and 1350 K, respectively. Figures 2(g) and 2(h) show how the R-point averaged sum and the Bethe's parameter σ change with the temperature. It can be seen that the order-disorder phase transitions of PMN and PCN occur around 1200 and 900 K, respectively, consistent with the known values from experiments [14,32,37]. Interestingly, Fig. 2(g) shows a sharp phase transition [unlike Fig. 2(e)], which is consistent with Ref. [19], while Fig. 2(h) shows that σ occupies the entire interval from zero to one, indicating that the system has continuously become more ordered (at least locally) as the temperature decreases from the melting point.

The approximation employed in Eq. (4) results from two considerations: (i) At high temperatures (∼1000 K) the Einstein or the Debye model [38] converges to the Dulong-Petit law since the Debye temperature of PMN is known to be less than 600 K [39–41], and that of PCN is expected to be even lower according to the Lindemann melting formula [42]. (ii) After the order-disorder phase transition at a rather high temperature [see Fig. 2(g)], no matter which equation is used for the kinetic energy, the system remains ordered, not affecting the predicted transition temperature. This approach indeed results in a satisfactory prediction of the order-disorder transition temperature.

In summary, using first-principles-based numerical simulations, we have shown that NNA is a key factor accounting for the compositional ordering in complex perovskite $Pb(BB')O_3$ even when the electrostatic energy is included. The analysis reveals that NNA is responsible for the formation of the β^{I} and β^{II} sublattices seen in PMN and PCN. In addition, we have found that the configuration degeneracy with respect to energy contributes to the partial order/disorder observed in $Pb(B_{1/3}B'_{2/3})O_3$. We hope that our study helps achieve a better understanding of the ordering in relaxor ferroelectrics of complex perovskite structure.

ACKNOWLEDGMENTS

This work is financially supported by the National Natural Science Foundation of China (NSFC, Grants No. 11974268, No. 11564010, No. U153721, No. 51911530121, and No. 12074304), the Natural Sciences & Engineering Research Council of Canada (NSERC, Grant No. RGPIN-2017-06915), and the US Office of Naval Research (ONR, Grant No. N00014-16-1-3106). L.L. thanks the support from Natural Science Foundation of Guangxi (Grants No. AA138162, No. GA245006, No. FA198015, and No. AA294014), and High Level Innovation Team and Outstanding Scholar Program of Guangxi Institutes. D.W. also thanks the support from China Scholarship Council (Grant No. 201706285020).

[1] O. Svitelskiy, J. Toulouse, G. Yong, and Z.-G. Ye, Polarized Raman study of the phonon dynamics in $Pb(Mg_{1/3}Nb_{2/3})O_3$ crystal, Phys. Rev. B **68**, 104107 (2003).

[2] K. Hirota, Z.-G. Ye, S. Wakimoto, P. M. Gehring, and G. Shirane, Neutron diffuse scattering from polar nanoregions in the relaxor $Pb(Mg_{1/3}Nb_{2/3})O_3$, Phys. Rev. B **65**, 104105 (2002)

[3] L. A. Bursill, H. Qian, J.-L. Peng, and X. D. Fan, Observation and analysis of nanodomain textures in the dielectric relaxor lead magnesium niobate, Physica B **216**, 1 (1995)

[4] A. A. Bokov and Z.-G. Ye, Recent progress in relaxor ferroelectrics with perovskite structure, J. Mater. Sci. **41**, 31 (2006).

[5] N. Setter and L. Cross, The role of B-site cation disorder in diffuse phase transition behavior of perovskite ferroelectrics, J. Appl. Phys. **51**, 4356 (1980).

[6] D. Wang and Z. Jiang, Dielectric response of $BaZrO_3/BaTiO_3$ superlattice, J. Adv. Dielectr. **6**, 1650015 (2016).

[7] A. A. Bokov, Compositional order-disorder in mixed ferroelectrics, Ferroelectrics **183**, 65 (1996).

[8] A. Al-Barakaty, S. Prosandeev, D. Wang, B. Dkhil, and L. Bellaiche, Finite-temperature properties of the relaxor $PbMg_{1/3}Nb_{2/3}O_3$ from atomistic simulations, Phys. Rev. B **91**, 214117 (2015).

[9] A. Bokov, V. Shonov, I. Rayesvsky, E. Gagarina, and M. Kupriyanov, Compositional ordering and phase transition in $Pb(Yb_{0.5}Nb_{0.5})O_3$, J. Phys. Condens. Matter **5**, 5491 (1993).

[10] A. A. Bokov, I. P. Raevskii, and V. G. Smotrakov, Influence of ion ordering at lattice sites on the properties of $Pb_2B'B''O_6$ ternary oxides, Sov. Phys. Solid States **25**, 2025 (1983).

[11] L. Bellaiche and D. Vanderbilt, Electrostatic Model of Atomic Ordering in Complex Perovskite Alloys, Phys. Rev. Lett **81**, 1318 (1998).

[12] M. J. Cabral, S. Zhang, E. C. Dickey, and J. M. LeBeau, Gradient chemical order in the relaxor $Pb(Mg_{1/3}Nb_{2/3})O_3$, Appl. Phys. Lett. **112**, 082901 (2018).

[13] S. Shetty, A. Damodaran, K. Wang, Y. Yuan, V. Gopalan, L. Martin, and S. Trolier-McKinstry, Relaxor behavior in

ordered lead magnesium niobate $PbMg_{1/3}Nb_{2/3}O_3$ thin films, Adv. Funct. Mater **29**, 1804258 (2019).

[14] P. K. Davies and M. A. Akbas, Chemical order in PMN-related relaxors: structure, stability, modification, and impact on properties, J. Phys. Chem. Solids **61**, 159 (2000).

[15] V. Polinger and I. B. Bersuker, Origin of polar nanoregions and relaxor properties of ferroelectrics, Phys. Rev. B **98**, 214102 (2018).

[16] C. Wang, Z. Fu, N. Zhang, M. Paściak, J. Zhuang, Z. Liu, W. Ren, and Z.-G. Ye, Determination of chemical ordering in the complex perovskite $Pb(Cd_{1/3}Nb_{2/3})O_3$, IUCrJ **5**, 808 (2018).

[17] C. G. F. Stenger and A. J. Burggraaf, Order-disorder reactions in the ferroelectric perovskites $Pb(Sc_{1/2}Nb_{1/2})O3$ and $Pb(Sc_{1/2}Ta_{1/2})O_3$: I. Kinetics of the ordering process, Phys. Status Solidi A **61**, 275 (1980).

[18] F. Nix and W. Shockley, Order-disorder transformations in alloys, Rev. Mod. Phys. **10**, 1 (1938).

[19] J. W. Christian, *The Theory of Transformations in Metals and Alloys* (Pergamon, Oxford, 2002).

[20] T. R. Welberry, *Diffuse X-Ray Scattering and Models of Disorder* (Oxford University Press, Oxford, 2010).

[21] D. Wang, J. Liu, J. Zhang, S. Raza, X. Chen, and C.-L. Jia, Ewald summation for ferroelectric perovksites with charges and dipoles, Comput. Mater. Sci. **162**, 314 (2019).

[22] K. Okhotnikov, T. Charpentier, and S. Cadars, Supercell program: a combinatorial structure-generation approach for the local-level modeling of atomic substitutions and partial occupancies in crystals, J. Cheminformatics **8**, 17 (2016).

[23] J. Enkovaara, C. Rostgaard, J. J. Mortensen, J. Chen, M. Dulak, L. Ferrighi, J. Gavnholt, C. Glinsvad, V. Haikola, H. A. Hansen *et al.*, Electronic structure calculations with GPAW: A real-space implementation of the projector augmented-wave method, J. Phys.: Condens. Matter **22**, 253202 (2010).

[24] H. J. Monkhorst and J. D. Pack, Special points for Brillouin-zone integrations, Phys. Rev. B **13**, 5188 (1976).

[25] M. Ernzerhof and G. E. Scuseria, Assessment of the Perdew–Burke–Ernzerhof exchange-correlation functional, J. Chem. Phys. **110**, 5029 (1999).

[26] P. Virtanen, R. Gommers, T. E. Oliphant, M. Haberland, T. Reddy, D. Cournapeau, E. Burovski, P. Peterson, W. Weckesser, J. Bright *et al.*, SciPy 1.0: fundamental algorithms for scientific computing in Python, Nat. Methods, **17**, 261 (2020).

[27] M. E. J. Newman and G. T. Barkema, *Monte Carlo Methods in Statistical Physics* (Oxford University Press, Oxford, 1999).

[28] V. A. Isupov, Ferroelectric and antiferroelectric perovskites $PbB'_{0.5}B''_{0.5}O_3$, Ferroelectrics, **289**, 131 (2003).

[29] A. A. Bokov, N. P. Protsenko, and Z.-G. Ye, Relationship between ionicity, ionic radii and order/disorder in complex perovskites, J. Phys. Chem. Solids **61**, 1519 (2000).

[30] R. D. Shannon, Revised effective ionic radii and systematic studies of interatomic distances in halides and chaleogenides, Acta Crystallogr. **32**, 751 (1976).

[31] B. P. Burton, Why $PbB_{1/3}B'_{2/3}O_3$ perovskites disorder more easily than $BaB_{1/3}B'_{2/3}O_3$ perovskites and the thermodynamics of 1:1-type short-range order in PMN, J. Phys. Chem. Solids **61**, 327 (2000).

[32] L. Farber, M. Valant, M. A. Akbas, and P. K. Davies, Cation ordering in $Pb(Mg_{1/3}Nb_{2/3})O3$-$Pb(Sc_{1/2}Nb_{1/2})O_3$ (PMN–PSN) solid solutions, J. Am. Ceram. Soc. **85**, 2319 (2002).

[33] H. Bethe, Order and disorder in alloys, J. Appl. Phys. **9**, 244 (1938).

[34] For $Pb(B_{1/2}B'_{1/2})O_3$, $\sigma = 2q - 1$ [9].

[35] L. D. Landau and E. M. Lifshitz, *Statistical Physics Part 1*, Course in Theoretical Physics Vol. 5, 3rd ed. (Pergamon, Oxford, 1980).

[36] Z. Li, Z. Xi, Z. Xu, H. Wang, and X. Yao, High temperature phase diagram of PMN-PT binary system, Ferroelectrics, **326**, 31 (2005).

[37] L. Farber and P. Davies, Influence of cation order on the dielectric properties of $Pb(Mg_{1/3}Nb_{2/3})O_3$-$Pb(Sc_{1/2}Nb_{1/2})O_3$(PMN-PSN) relaxor ferroelectrics, J. Am. Ceram. Soc. **86**, 1861 (2003).

[38] C. Kittel, *Introduction to Solid State Physics*, 8th ed. (John Wiley & Sons, New York, 2004).

[39] M. V. Gorev, I. N. Flerov, V. S. Bondarev, and Ph. Sciau, Heat capacity study of relaxor $Pb(Mg_{1/3}Nb_{2/3})O_3$ in a wide temperature range, J. Exp. Theor. Phys. **96**, 531 (2003).

[40] Y. Moriya, H. Kawaji, T. Tojo, and T. Atake, Specific-Heat Anomaly Caused by Ferroelectric Nanoregions in $Pb(Mg_{1/3}Nb_{2/3})O_3$ and $(Mg_{1/3}Ta_{2/3})O_3$ Relaxors, Phys. Rev. Lett. **90**, 205901 (2003).

[41] S. N. Gvasaliya, S. G. Lushnikov, Y. Moriya, H. Kawaji, T. Atake, M. B. Smirnov, and V. Y. Kazimirov, Specific heat of cubic relaxor ferroelectrics, J. Phys.: Condens. Matter **16**, 8981 (2004).

[42] J. M. Ziman, *Principles of the Theory of Solids*, 2nd ed. (Cambridge University Press, Cambridge, 1972).